SPATIO-TEMPORAL VARIATION OF AEOLIAN SHOREWARD SAND TRANSPORT MEASURED USING NEAR-CONTINUOUS LASER SCANNING

Sander Vos[1], Katharina Anders[2], Alain de Wulf[3], Sierd de Vries[4] and Roderik Lindenbergh[5]

A beach in Mariakerke-Bad (Belgium) was monitored in 2017-2018 for more than a year with a near-continuous laser scan system. From a total of 8500 scans 7700 hourly scan epochs were used to study the spatio-temporal shoreward sand transport at the beach. In order to account for weather influences and other possible disturbances of the scan-system, a time-dependent correction method was applied to reduce rotation errors up to 0.2 degrees in the point cloud orientation (around the zero point of the laser scanner) reducing height errors on the beach to the order of centimeters. Cross shore analysis of the beach profile shows that shoreward transport occurs at most times during the year with an accumulated maximum of 17m3/m throughout the measurement period and maximum transport rates of 0.6 m3/m/day. However most of the shoreward sand transport is redistributed seawards again due to beach shaping leaving a total of about 2 m3/m a year which is below the average values found along the Belgium coast. The spatio-temporal behavior of the shoreward sand transport has been studied with the 4D-OBC analysis technique which identified accumulations of sand in the full 4D point cloud dataset. A total of about 3600 4D-OBC accumulation events were identified and most found accumulations on the beach can be associated with natural (aeolian) processes. Also, accumulations appear to occur during the whole year which is consistent with the previous cross-shore analysis.

Keywords: beach; aeolian transport; permanent laser scanning; spatio-temporal data analysis

INTRODUCTION

Sandy coasts constitute about 34% of all coastal areas in the world (Hardisty, 1994). At present already about 25% of these beaches are eroding (Luijendijk et al., 2018) and 50% are likely to experience coastal squeeze before the next century (Vousdoukas, 2020) due the expected climate change trends (IPCC, 2022). A large part of coasts which are not artificially maintained will depend on natural processes such as shoreward sand transport to adapt to the expected sea level rise and maintain their safety and resilience.

Shoreward sand transport is highly dynamic in nature, partly event-driven and dependent on marine and aeolian forcing like wind speed, local morphology and properties (Hesp, 1999). Tides and waves transport sand toward the high waterline during mild conditions (Vos et al., 2020). Here aeolian (i.e. wind-driven) processes transport the sand towards the dunes (Duarte-Campos et al., 2018 and Hoonhout and de Vries, 2017) where e.g. vegetation traps the sand (Buckley, 1996 and Valentini et al., 2020) strengthening the dunes and increasing coastal protection. This study will focus on the aeolian part of the shoreward sand transport as this area is covered with the used measurement system.

Aeolian shoreward transport depends on local (weather) conditions and on sediment availability (Hoonhout and de Vries, 2016), i.e. the amount of transportable sand, determined by the rheological properties of sand, such as humidity (wiggs et al., 2004 and Swan et al 2021), grain size distribution (Arens et al., 2002 and Hateren et al., 2019) and soil type (Strypsteen, 2021a). All these actors interact on various spatio-temporal scales which requires arduous measurements to obtain more information of all of these actors.

Often transport rates and the long-term effect on dunes can be/are estimated on available data from short-term field campaigns (Campos et al., 2019, Goosens et al., 2018 and Strypsteen et al., 2021b) in the order of days/weeks and/or long-term datasets (Brody et al., 2019, Strypsteen et al., 2019 and Vries et al., 2012) in the order of years. However information in the intermediate spatio-temporal scale linking the short-term field campaigns and long-term datasets is still missing. Especially event-driven phenomena and anthropogenic effects are so far hard to quantify. A better understanding of these processes can help safeguard our coasts with respect to future climate change and further improve the available numerical models for long-term forecasting.

Video based systems (Holman and Stanley, 2007) have been the main technique to study/observe beach dune dynamics (Hage et al., 2018a, b and Smit et al., 2007) over longer spatio-temporal scales in the last decades. Since about six years high-resolution near-continuous terrestrial laser scanning (TLS) has been available to provide spatially accurate measurements at high temporal and spatial resolution

[1] Department of Civil Engineering and Geosciences, Delft, University of Technology, Stevinweg 1, 2628 CN, Delft, The Netherlands, s.e.vos@tudelft.nl
[2] Institute of Geography, Heidelberg University, Im Neuenheimer Feld 368, 69120, Heidelberg, Germany, katharina.anders@uni-heidelberg.de
[3] Department of Geography, Ghent University, Krijgslaan S8 281, 9000, Gent, Belgium, alain.dewulf@ugent.be
[4] Department of Civil Engineering and Geosciences, Delft, University of Technology, Stevinweg 1, 2628 CN, Delft, The Netherlands, sierd.devries@tudelft.nl
[5] Department of Geoscience and Remote Sensing, Delft, University of Technology, Stevinweg 1, 2628 CN, Delft, The Netherlands, r.c.lindenbergh@tudelft.nl

(here hourly) of the beach surface (O'Dea et al., 2019 Deruijter et al., 2020 and Vos et al., 2017 and 2022).

Near continuous TLS provides large scale 4D points clouds with easily more than 1e10 3D points. (Vos et al., 2022). This poses challenges in determining surface properties over the multiple spatiotemporal scales. The main challenge in identifying sand transport in dense 4D point clouds is that there is no a-priori knowledge about the timing and spatiotemporal properties of sand transport. We use a time series-based method of change detection to identify time spans where temporary accumulation of sand occurs, i.e. local surface increase followed by decrease. This corresponds to sand that is transported to a location and later removed, e.g., due to cleaning or aeolian transport. Once temporary accumulation is detected at locations in the scene, its spatial extent is delineated via segmentation of all neighboring locations with a similar surface change history of temporary accumulation. A spatiotemporal region growing algorithm is used to extract so-called 4D objects-by-change (4D-OBCs; Anders et al., 2020). Identified 4D-OBCs can be used to characterize sand transport in its spatial and temporal properties, such as the timing and the volume of transported sediment.

In this study, a 400-meter long beach in Belgium was monitored for one year with near-continuous terrestrial laser scanning to gain more insight on shoreward sand transport on the beach. Both 1D and 4D analysis techniques were used to determine the (spatio-temporal aspects of) shoreward sand transport for up to a year.

FIELD LOCATION MARIAKERKE BAD

Field site description

A one-year hourly 4D-pointcloud dataset was acquired at the sandy coast of Mariakerke Bad , Belgium (51.21˚N, 2.87 ˚ E) (see figure 1). Measurements were obtained with a Riegl VZ-2000 laser scanner mounted on top of Hotel Vajamundo at a height of about 40 meters above mean sea level. The practical range is about 600 meters with a usable scan area of about 200*400 meters. The laser scanner was placed on a three-legged iron pole (mounted against the wall) which was cross-braced to minimize horizontal displacements. The scanner was protected with a double PVC (Polyvinyl Chloride) housing to avoid fouling and temperature extremes potentially affecting the laser scanner. Scans were initiated by a command computer stored inside the hotel.

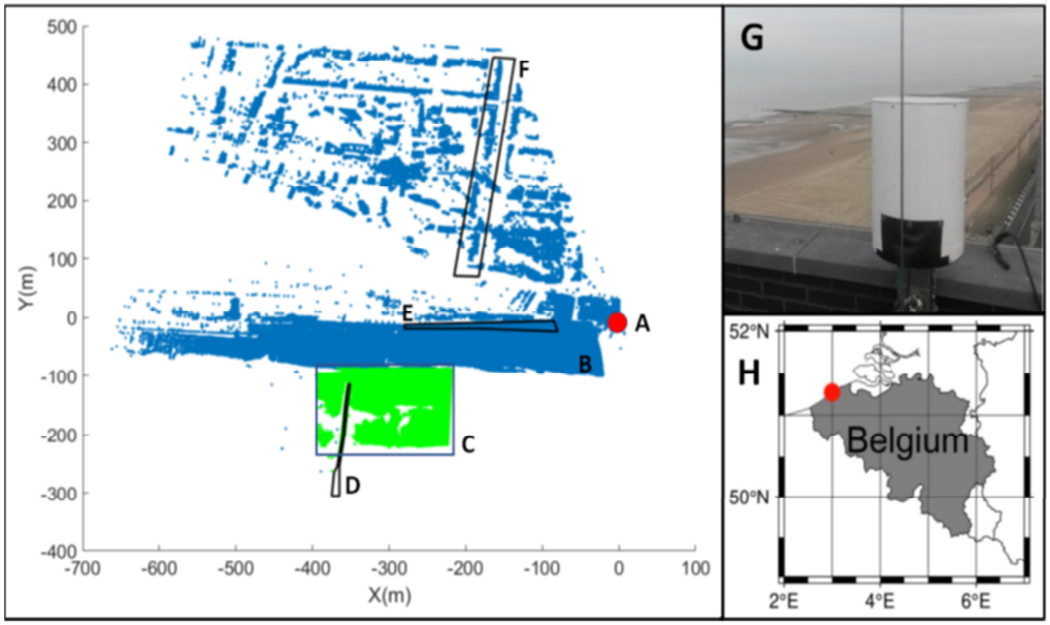

Figure 1: Example of a typical scan of the beach acquired by the laser scanner (A, G) overlooking the beach at Mariakerke Bad, Belgium (H). The scan shows a typical high (B) and low (C) water scan with the three georeference areas ((D) groin, (E) seawall and (F) street) studied for the time dependent corrections.

The beach at Mariakerke Bad is orientated from the southwest to the northeast. The beach is subject to a macro tidal range between 3.5 and 5 meters (Brand et al., 2019) and mostly westerly waves (significant wave height between 0.5-3 meters). The intertidal area is about 150 meters with a berm of about 50 meters before the seawall. The coast is protected by a seawall behind the beach and groins around the waterline which are flooded during high water. Beach maintenance is performed regularly with small-scale beach nourishment and beach shaping. In the measuring period no nourishments were performed. Beach shaping was performed several times during the measuring period whereby the beach was completely flattened for the first 40-50 meters from the seawall.

Available data

Scan data was acquired over a 392-day time period from the 9th November 2017 till 6th December 2018. Scans were acquired hourly with several gaps due to technical problems resulting in a total of about 8.500 available scans. The total uptime is shown in figure 2. Due to weather related problems (like rain and fog) about 7.770 scan epochs were usable for further analysis.

During the first month, hourly scans were made over a 200 degrees window (at 0.03˚*0.03˚ resolution) covering part of the city. Due to processing concerns of the large data files the scan window was reduced to 110 degrees only covering the seawall and beach area. This however limited the possibilities for using the internal inclination sensor and necessitated extra corrections for the time-dependent corrections.

Hourly wind data like wind direction and speed (see figure 2) were obtained online from the Meetnet Vlaamse Banken (2022) from Nieuwpoort (about 15 kilometers southwest of Mariakerke Bad), the nearest available location in Nieuwpoort.

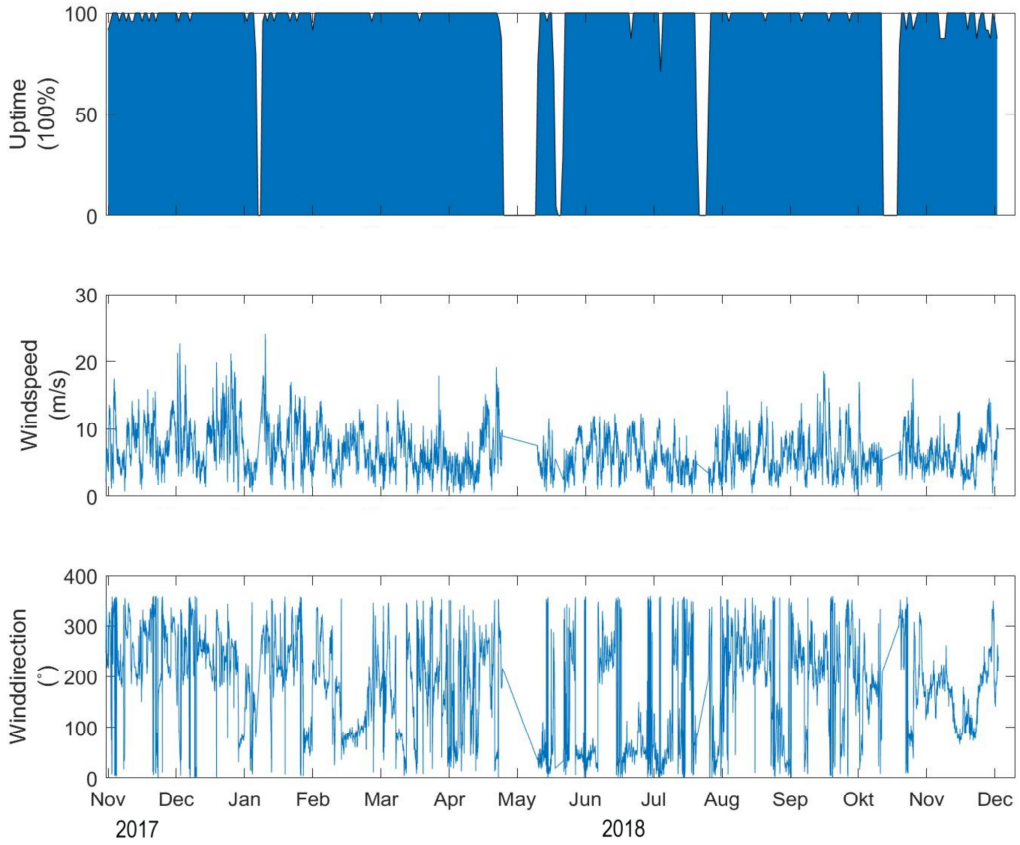

Figure 2: Available laser scan epochs during the measuring period. The uptime (in %) is defined as the percentage of the daily hourly scans (i.e. 50% means 12 scans for an 24 hour period). Wind data (windspeed and -direction) was obtained from the nearest available weather location Nieuwpoort.

DATA PROCESSING METHODS

Laser scan corrections

The global conversion matrix (local to Belgium Lambert 72 coordinates) was obtained by comparing the first scans with GNNS georeferenced reflectors and airborne lidar data (Sloover, 2019) of the groin (Figure 1D) and seawall (1E) in front of the hotel. For the time dependent corrections global reference data was reverse transformed to local coordinates of the laser scanner.

Permanent laser scanning over long time periods inhibit small oscillations (Kuschnerus et al., 2021) that result in artificial surface height variations at the beach. Georeferenced objects in the laser scan field of view are used to adjust for these small offsets. In Mariakerke Bad three possible objects have been investigated; the groin on the beach, the seawall (Figure 1D-1F) and buildings in the city. The groin on the beach seems the most obvious for corrections into the direction of the beach, but due to the tidal range whereby the groin is flooded during high water the groin was less usable. Time dependent corrections based on the groin showed large variations in corrections. Another obvious choice would be the city behind the beach, but a change in the scan settings after about one month made this area less usable. In the end the sea wall in front of the laser scanner resulted in the most stable time dependent corrections with the smallest variations.

For the corrections, a correction scheme modified from Sloover et al. (2019) is used. Individual laser scan epochs are corrected by comparing a fixed object in the N^{th} scan epoch with the first scan epoch and rotating (calculating the rotation angle around the X- and Y axis) the scan by minimizing the vertical distance between the scan data in the georeferenced areas (Figure 1D-1F) in local coordinates:

$$\begin{cases} (\Delta\Phi, \Delta\Psi) = minimise\ (J) \\ J = \sum (Z_{scan} - Z_{obs})^2 \end{cases} \quad (1)$$

with $\Delta\Phi$, $\Delta\Psi$ the angle corrections around the X- (towards the sea) and Y-axis, J the cost function and Z_{scan} and Z_{obs} the height difference of the reference objects (within the areas 1D-1F).

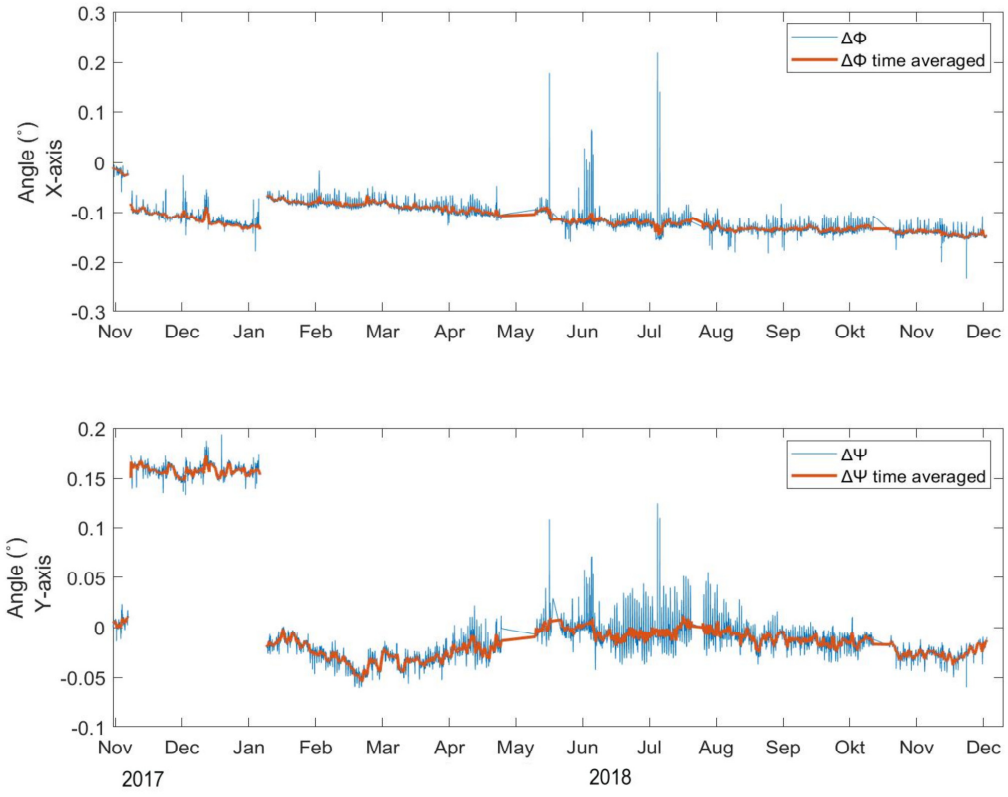

Figure 3: Time-dependent angle corrections for the X- (ΔΦ) and Y- (ΔΨ) axis. The plots show the individual calculated time-dependent corrections and the time-averaged results.

The height of a point in the N^{th} scan epoch was compared with the nearest point in the first scan epoch with a maximum distance of 10 centimeters in the horizontal.

In order to account for errors in the georeference object detection (in the scan epochs) angle corrections larger than 0.2 degrees were ignored. Errors occur for example with erroneous removal of antropogenic objects (like people, trams, tramlines) on top of the seawall and situations where the seawall is not clearly visible in the scan epochs due to reflection errors (for example due to wet surfaces or fog).

The found corrections are shown in figure 3 showing the found rotation corrections around the X- and Y-axis with rotations up to 0.2 degrees. Although the laser scanner frame is bolted to a wall there was still room for small rotations of the laser scanner. It is not clear what caused the variations, but small errors could be detected and corrected. The resulted corrections reduced the average vertical error of the beach height to a couple of centimeters.

For the 1D analysis in the cross shore and alongshore direction an area of about 40*400 meters of the berm of the beach (where aeolian transport is expected to occur) on the northwest side of the laser scanner was considered. Initially the seawall was also considered for analysis as accumulations of sand are clearly visible, but distinguishing the sand accumulation on the seawall from other anthropogenic factors like people, trams and cars proved to be difficult.

4D-OBC clustering

Timespans and areas of sand transport are identified using spatiotemporal segmentation of 4D-objects by change (4D-OBCs, Anders et al., 2020). 4D-OBCs are extracted by identifying locations in the scene (i.e. changes on the beach) expressing temporary accumulation in their time series of surface change to determine the timing and duration of temporary sand accumulation without a-priori knowledge on its occurrence. Subsequently, the identified surface activity is spatially delineated as areas of similar surface change history, i.e. similar behavior of temporary accumulation in the identified timespan of a location. This change detection and delineation analysis is performed for all locations in the scene, so that all individual occurrences of temporary accumulation can be identified without any definition about the expected location or timing (Anders et al., 2021).

To perform this spatiotemporal segmentation, surface changes in the 4D point cloud data needs to be accessible in the spatial and temporal domain. The data structure of a space-time array is created for this, which is a 3D array where each 2D location represents a spatial location in the scene, and the 1D time series of surface changes is contained in the third dimension. This array is obtained by calculating surface change for each point cloud to the first point cloud in the time series, the null epoch. We derive surface change via direct point cloud comparison using the M3C2 algorithm (Lague et al., 2013). The distance from a point cloud epoch to the null epoch is calculated as purely vertical distance, where the vertical position is averaged among all local 3D points within a neighborhood radius of 0.5 m. This position averaging is performed for a set of regular 2D locations with 0.5 m spacing, so that a grid structure of the same locations is obtained for each epoch. By stacking these epochs of surface changes along the temporal domain, the space-time array is obtained, which allows direct access to the time series of surface changes at each location.

The space-time array is used to search for temporary sand accumulation at all locations in the observed scene. Temporary accumulation at a location is identified by first detecting change points in the time series of one location. A change point is detected as epoch when the time series changes with respect to the rolling median in a temporal window of 6 h. Once a change point is detected, the duration of the surface activity is determined as the timespan until the surface increase in the time series is reverted to the height at the start of the change. For details on the method of identifying temporary surface change in 3D time series, we refer the reader to Anders et al. (2021).

After this temporal change detection, spatial delineation is performed following the method as presented in Anders et al. (2021). The result of this region growing segmentation provides a set of 4D-OBC objects which experienced similar surface changes during the determined timespan in the delineated spatial extent. The object in its temporal and spatial extent is hence defined by its surface change history.

Figure 4 shows an example 4D-OBC consisting of a timespan of surface changes (left panel) and an area of spatial coverage (right panel) with the found accretion indicated between red lines. Around the 28th April 2018 an area with sediment accretion was detected in the middle part of the scan area. The area was about 70 by 10 meters with an accumulation height of about 10 centimeters. Looking at the local morphology in the right panel this area corresponds to a sand strip of about 10 centimeters height.

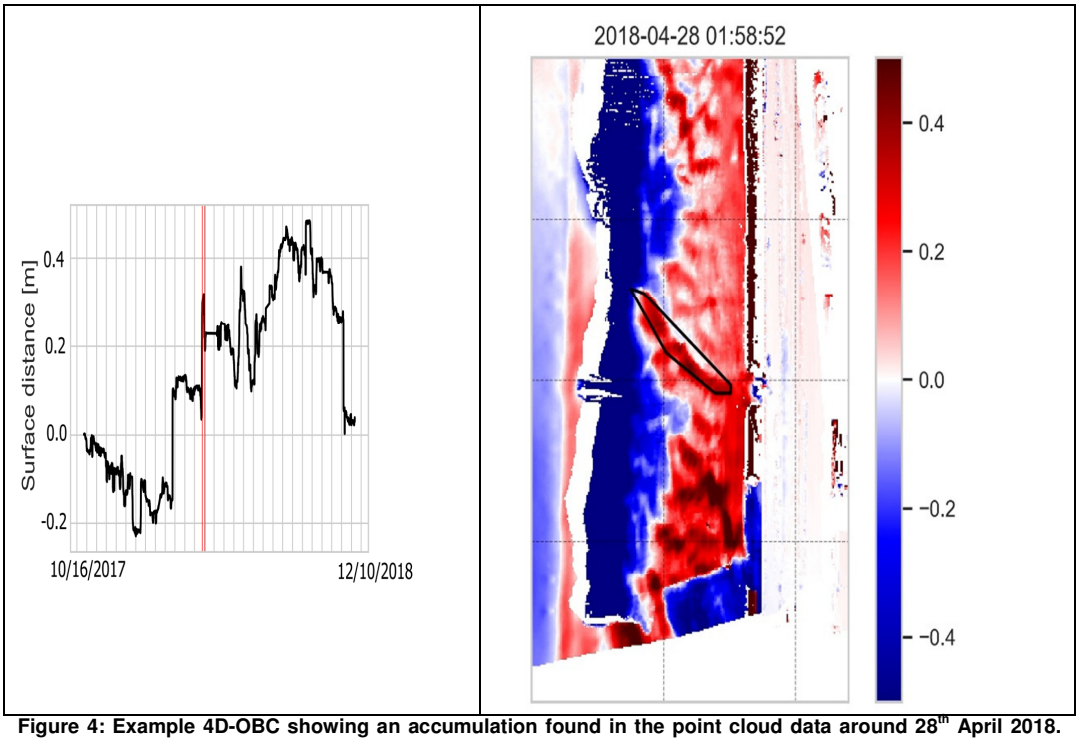

Figure 4: Example 4D-OBC showing an accumulation found in the point cloud data around 28th April 2018. The left graph shows the height difference timeline with the temporary peak found between red lines. The accumulation area is shown in the right graph indicated with a black encirclement. Colors in the right graph indicate surface height changes in meters.

POINTCLOUD ANALYSIS

1D cross-shore and alongshore analysis

Figures 5 and 6 show the results of the 1D cross-shore and alongshore analysis. It shows the cross-shore and alongshore accumulative beach volume changes of part of the beach over the whole measurement period in 2017 and 2018. The beach area is 40*400 meter in front of the seawall. A cross-shore profile of 40 meters from the seawall was selected to minimize the effect of the intertidal area in the analysis (i.e. the effect of marine processes was minimized). The presented volumes are calculated along one axis and averaged along the opposite axis meaning that results for the cross-shore analysis are average along alongshore axis and vice versa. The beach volumes are calculated by subtracting the beach surface heights of the N^{th} scan epoch from the first scan epoch at the same location.

Figure 5 shows the evolution off the cross-shore profile with accumulations shown in read and erosion shown in blue.. A slow accumulation of sand is visible in front of the seawall (around x=-30 meter) in the first two months filling up the ditch which was created just before the measuring period during the beach reshaping (The beach was reshaped on the 7^{th} of November 2017). The beach also retains a more natural profile (not shown here) after the beach flattening just before the start of the measuring period. Smaller scale beach profiling (i.e. not affecting the whole measurement area) in January and March 2018 (indicated with dashed lines) results in a partly redistribution of sand volume towards the sea (x<-75 meter). After that period the sand volumes slowly grow towards the end of November when a reflattening of the beach in November 2018 redistributes the sand back to the whole berm area.

Figure 6 shows the alongshore distribution of the total cross-shore volume over time (with y=0 towards the southwest and increasing y values towards the northwest). The plot shows local variations alongshore of the total cross-shore volume with a ‘wave length’ of about 10-30 meters and volume variations of 10-50 m3. The figure shows marginal volume variations in the y direction over time indicating that most volume accumulations are towards the seawall (as indicated in figure 5) with limited sand transport in the along shore direction.

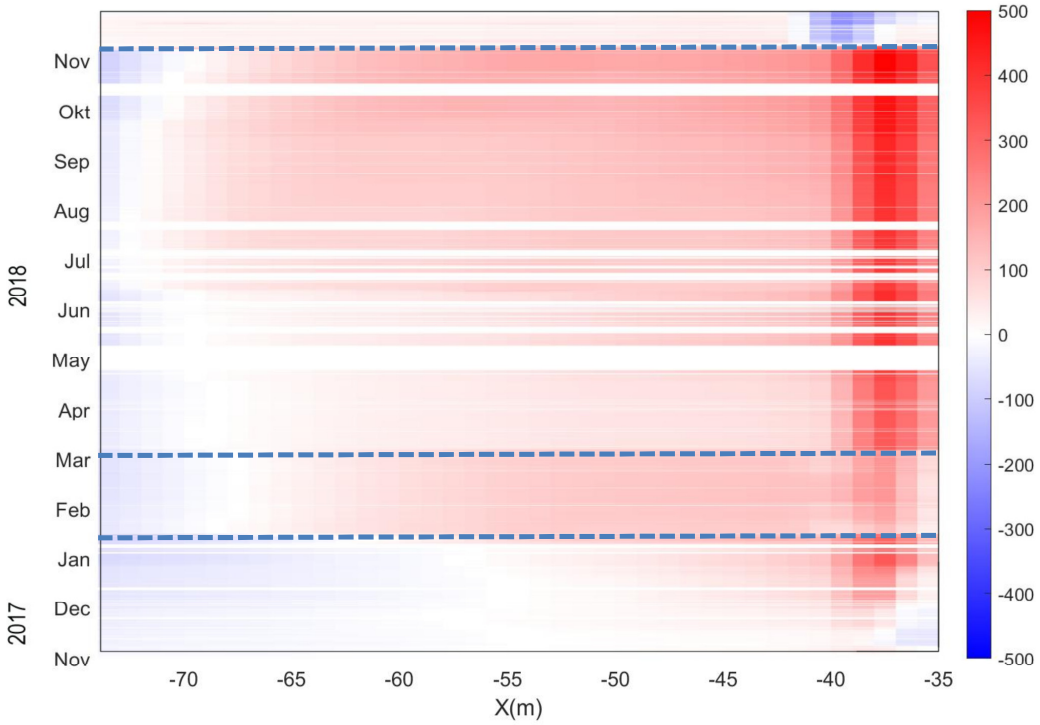

Figure 5: Cross-shore distribution of the along shore accumulative beach volume changes along the 400-meter of beach over the measurement period (accumulation is shown in read and erosion is shown in blue, both in m^3). Beach volumes are calculated by subtracting the beach heights from the first scan epoch from the N^{th} scan epoch. The seawall is around x=-30 m and the intertidal area is x<-75 m. Dashed blue lines indicate beach shaping activities and white horizontal stripes indicate no data.

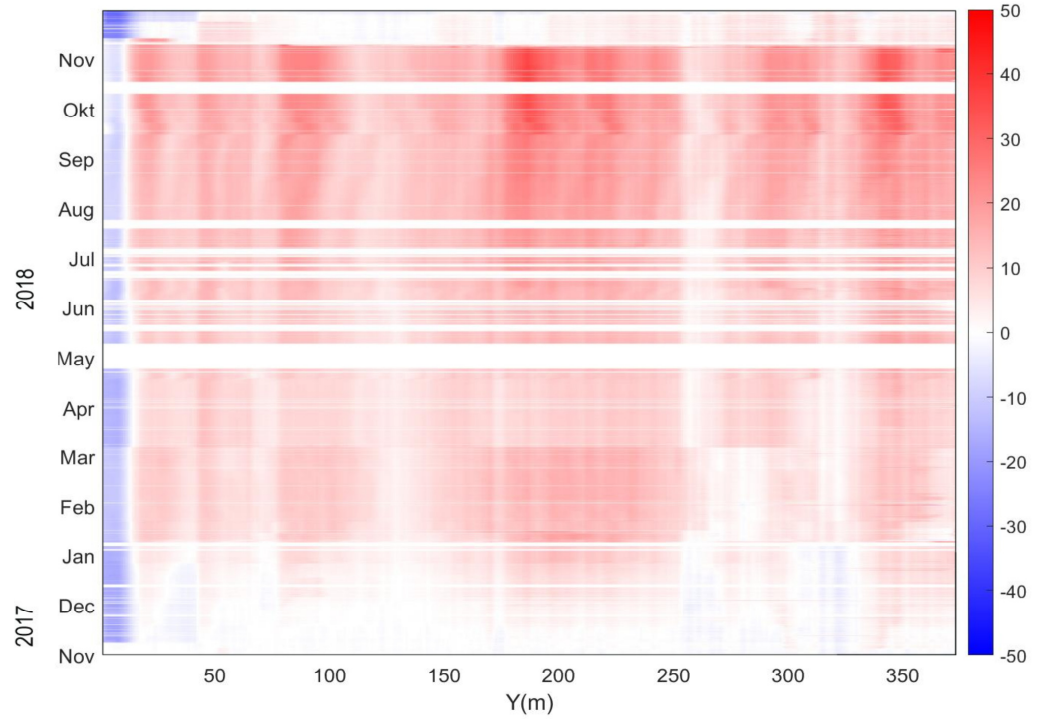

Figure 6: Along shore distribution of the cross-shore accumulative beach volume changes of the beach over the measurement period (accumulation in read, erosion is blue [both in m^3] and white stripes indicate no date). Beach volumes are calculated by subtracting the beach heights from the first scan epoch from the N^{th} scan epoch.

Shoreward sand transport

In order to obtain an idea of the total shoreward transport in Mariakerke-Bad figure 7 shows the total volume above the first scan epoch (which consisted of a flattened beach) along the cross-section over time. The volumes are averaged (over the alongshore) to m3 per linear meter. The plot shows the individual calculated volumes as a scatter plot and a time averaged line (over 24 hours) showing the long-term trend. The plots show a gradual increase of accumulated sand up to 17-18 m3/m until the beach reshaping in November 2018 reduces it to about 1-2 m3/m.

In the total shoreward sand transport there are several reductions visible (around the beginning of November, 2017, and February and March 2018) in the total volume. These are caused by either beach reshaping (in March 2018) or due to tidal influence at the edge of the scarp. This last case is illustrated in figure 8 (upper panel) which shows the beach evolution over the first 30 days over a somewhat longer stretch of beach (here 60 meters). To the right of the plot it shows the ditch slowly filling up while to the left the shoreward movement of the scarp is visible.

The volume plot in figure 8 shows the total volume change above ($Vol_{up)}$ and below (Vol_{down}) the first beach profile of 9th November 2017 and the total volume change of the bed between X=-35 till X=-90. The volume above the profile is calculated the same way as the volume in figure 7 (i.e. the volumes are averaged to m^3 per linear meter.) and the volume below the profile is calculated in a similar way only adding all volume changes below the height of the first profile. It shows that the Vol_{down} decreases faster than the Vol_{up}. indicating that more sand is disappearing on the scarp side than is accumulated in the ditch.

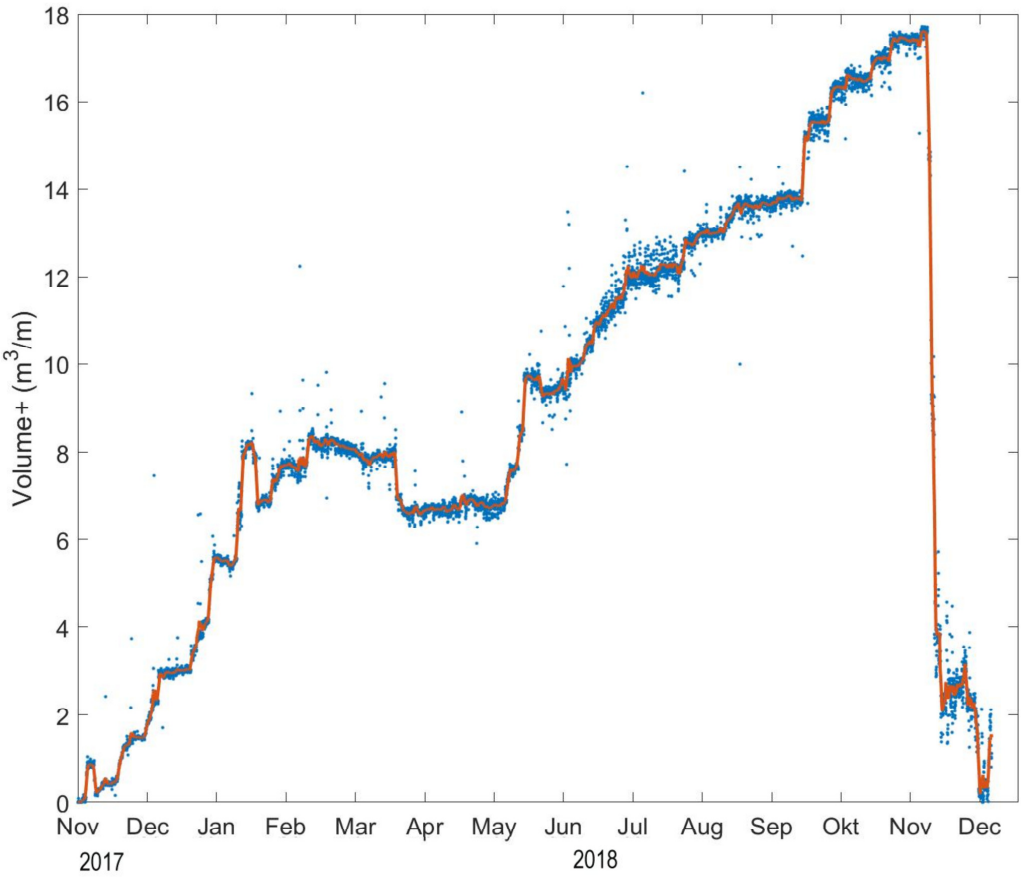

Figure 7: Averaged sand volumes (along the alongshore axis) in the berm above the first reference scan (consisting of a flattened beach) in m^3/m over the measuring period. The scatter plot shows individual volumes with the red line showing a time averaged trend (averaging period 24 hours). Points around July 2018 show a large scatter due to problems with the time dependent corrections.

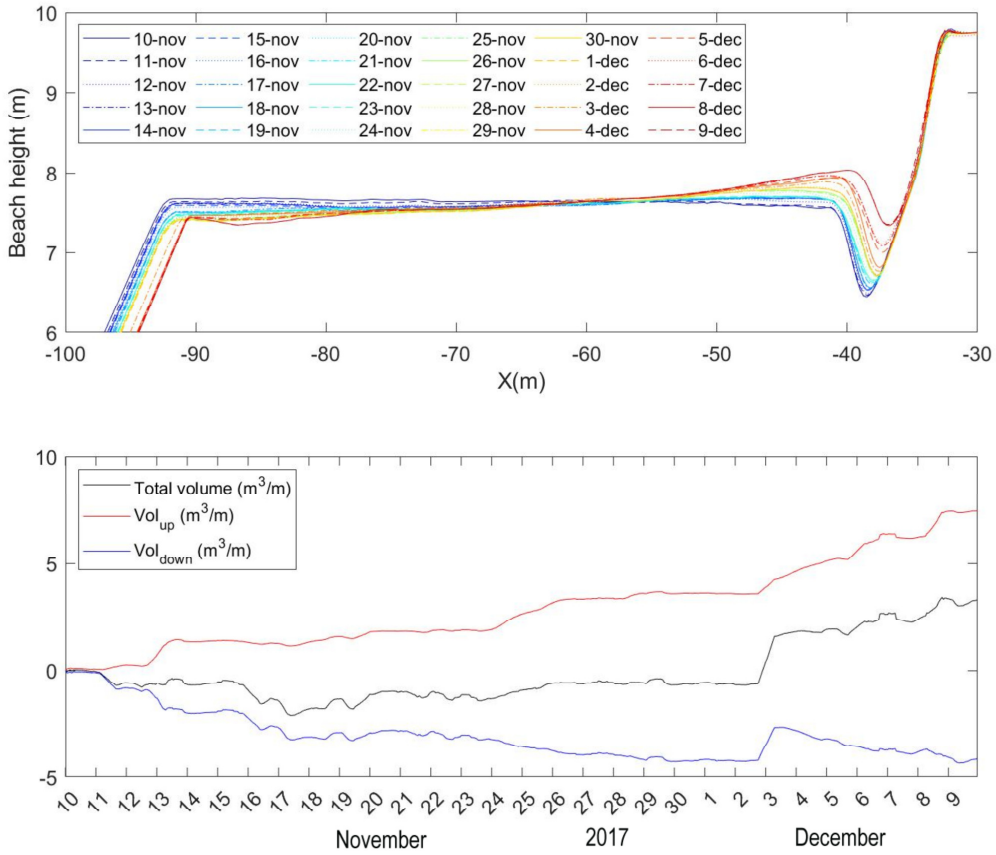

Figure 8: Top panel: Cross-shore beach height evolution over the first month (10th.November till 9th December 2017). Lower panel: Calculated volume below and above the height profile of the first day and the total volume change in the area from X=-35 to X=-85.

If all shoreward sand transport would be aeolian it would be expected that the total volume in this part of the beach would be zero or larger than zero (in case when sand is blown in from below the scarp). The total volume in figure 8 however shows a decreasing trend indicating that other processes (like wave attack on the scarp) influence the sand transport and transport sand towards the sea. This is also visible in the top panel where the scarp on the left moves shoreward.

When the alongshore sediment transport is much smaller than cross-shore sand transport, the change in bed height and the cross-shore sand transport can be estimated using the 1-dimension mass continuity equation as expressed in equation 2:

$$\frac{\mathrm{dh}}{dt} = \frac{S_x}{1-\phi} = \frac{1}{1-\phi}\frac{\partial Q_x}{\partial x} \qquad (2)$$

where h represents the height of the bed at a certain time, S_x the sedimentation/erosion rate, and Q_x the cross-shore sand transport at a specific location along the cross-section. The porosity ϕ is assumed constant and equal to 0.4. The cross-shore transport at a certain point is obtained by integrating the height changes in time along the profile. Here the profile is integrated from X=-37m (as the profile is constant as can be seen in figure 8) towards the sea.

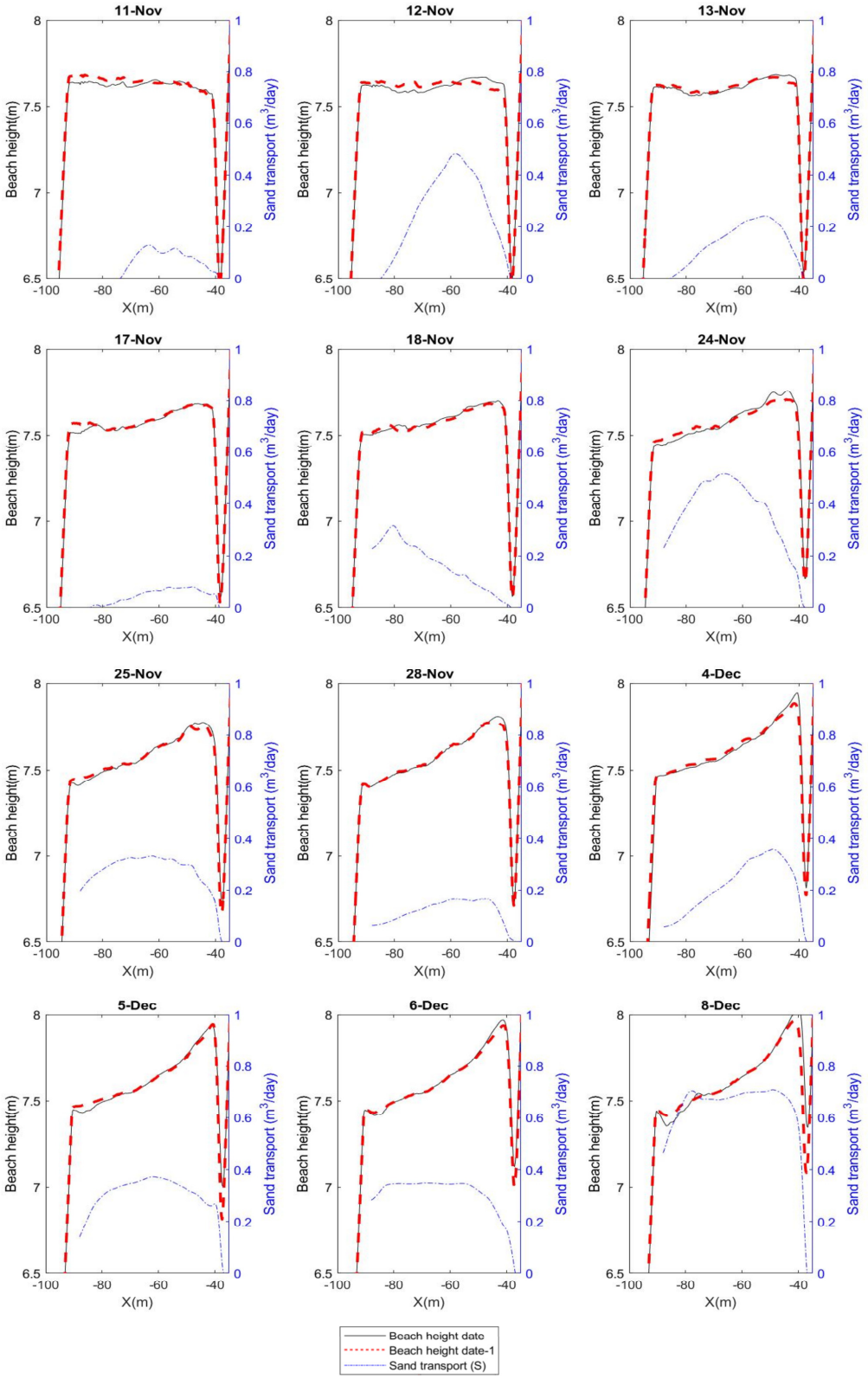

Figure 9: Estimated cross-shore sand transport (Q_x) based on formula 2 for days that sand transport could be identified (blue dashed line). Next the plots show the beach profile for the date specified in the title (black line) and the beach profile of the day before (dashed red line).

Figure 9 shows the calculated cross-shore sandtransport per day towards the coast (with positive values indicating shoreward sand transport) based on formula (2) for days that sand transport could be idenditifed. The identification of the days was done manually and was determined on the beach profiles changes. The plot shows that transport rates increase at all dates towards the coast with a maximum around 10-30 meter of the ditch (between X=-45m and X=-65 m). Values up to 0.6 m^3/day can be observed with a maximum transport rate about 10-30 meter before the ditch. All profiles have positive values on the scarp side of the profile indicating that sand is transported from below the scarp towards the coast.

4D-OBC analysis

In the measurement period in 2017 and 2018 around 3.600 4D-OBCs were found. Figure 10 and 11 show statistics of this analysis. The figure 10 upper plots show the histograms of the height and volume parameters of the 4D-OBCs. It shows that most 4D-OBCs have a height change of less than 10 cm with volumes less than 1 m^3 which is consistent with aeolian sand transport. Larger 4D-OBCs are more likely be connected with anthropogenic activities like presence of humans or cars on the beach or other activities. The lower plots in figure 10 show the distribution of the found 4D-OBCs over time. The 4D-OBCs are reasonably distributed over the year. This is in line with the results found in figure 5 which shows the identified shoreward accumulation on the beach at Mariakerke-Bad.

Figure 11 shows the wind conditions during the periods of the found 4D-OBCs. The left upper plot shows that most 4D-OBC's are related with average wind-speeds above 6-7 m/s while the period that the wind speed is above aeolian wind conditions (this border has been deduced from Vries, 2012(b) which shows that aeolian sand transport start around 7 m/s) varies between 0 to almost 100% of the time of the 4D-OBC. The main wind direction is 200 degrees which is a seaward wind direction at our study site. These 4D-OBJs are probably connected to the anthropogenic activities on the beach. The wind direction variability during the occurrence of the 4D-OBC does not show a clear pattern in our analysis.

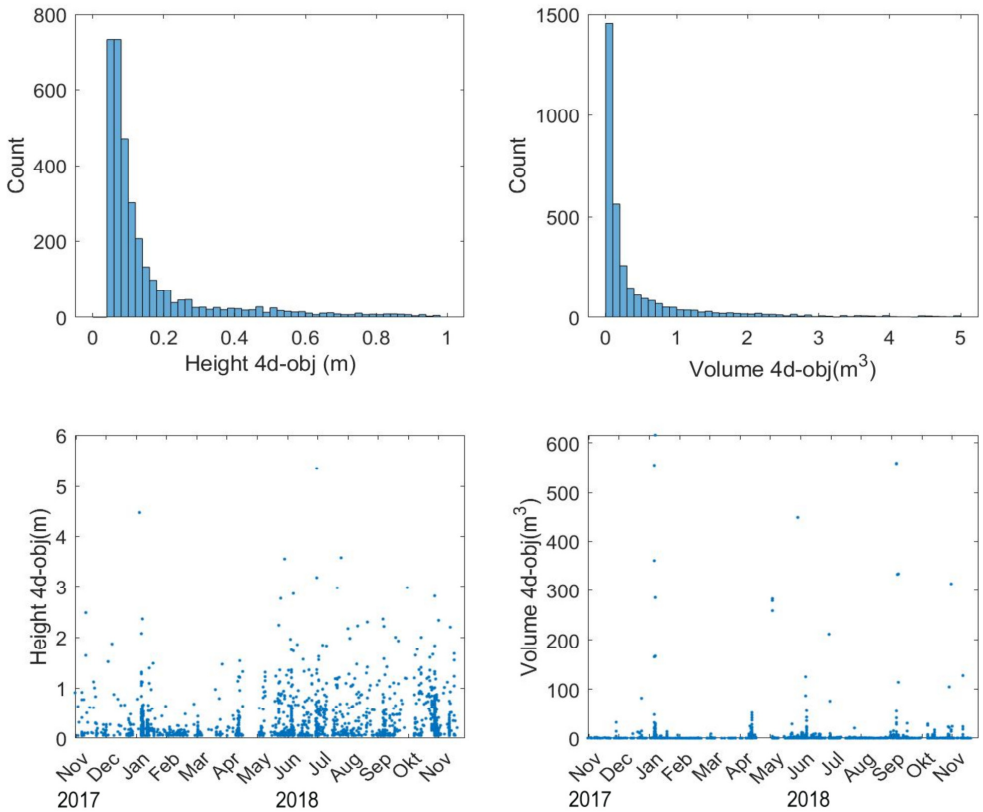

Figure 10: Result of the 4D-OBC analysis. The upper plots show histograms of the height and volume (size*height) of the different 4D-OBS's. The lower plots show the distribution over time of the same parameters.

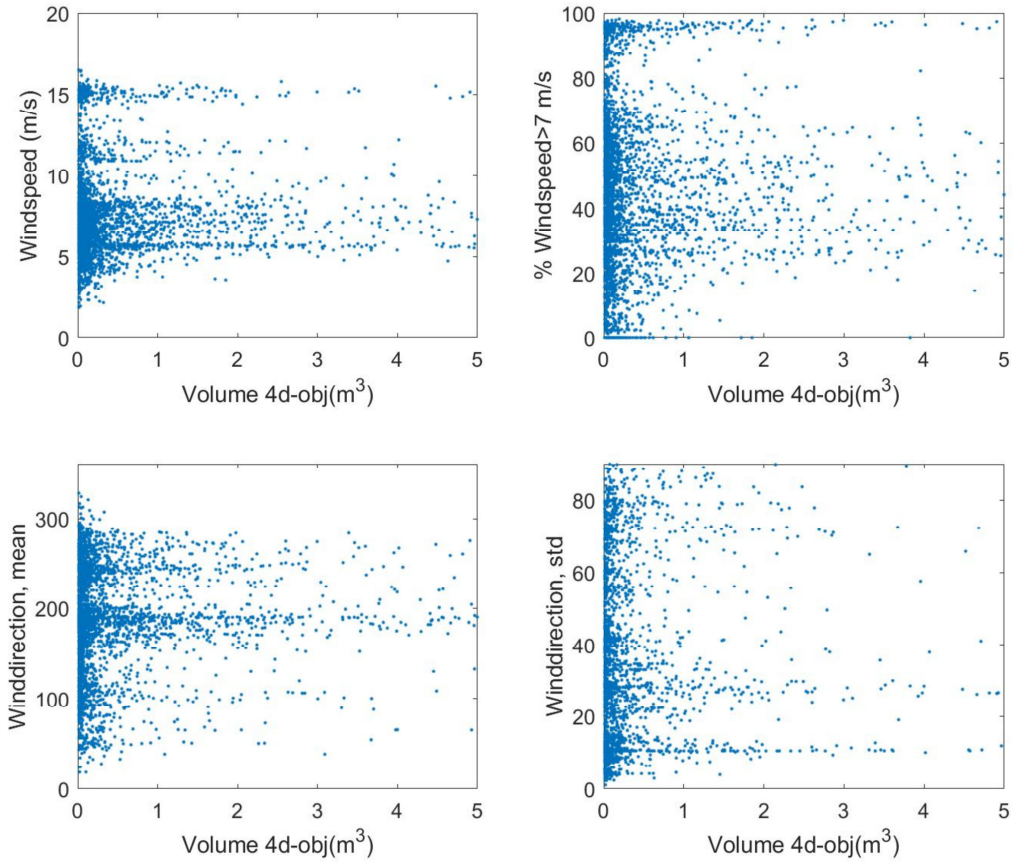

Figure 11: Wind conditions during the observed 4D-OBCs. The left upper plot shows the average wind speed versus the observed 4D-OBC volumes while the right upper plot shows the percentage of the time that the wind speed was above 7m/s. The lower plots show the mean wind direction and the wind-direction variability (expressed in the standard deviation) during a 4D-OBC.

DISCUSSION

The large amount of near-continuous TLS data poses a challenge in processing and extracting all the relevant information at the beach of Mariakerke Bad. The number of usable georeferenced objects in the area is limited and ultimately only one object (i.e. the seawall) could be used to obtain stable results in the cross-shore direction of the beach. The inclusion of the groin in the reference data increased the variability of the results due to the changing visibility of the groin in the 3D point clouds due to tidal flooding.

The time-dependent correction method is a simplified version of the method developed by Sloover et al. (2019). This method obtained higher accuracy corrections (in the order of millimeters vs centimeters) on a smaller subset of the whole dataset, but the method is a couple of times slower than the simplified version which had the preference with the whole dataset. In a previous measurement campaign with the near-continuous laser scanner in Kijkduin, The Netherlands (Vos et al., 2022) an iterative closest point method (Besl & McKay, 1992) was applied for correction. This method proved less usefull for the data in this study as solutions had a tendency of large translations which shifted the position of the pointcloud (ie the position of the laserscanner). As the laserscanner was bolted to a wall and known not to move this method did not support the time-dependent correction.

Quantitative results show shoreward sand transport occurring distributed over the year with maximum accumulated volumes up to 17 m^3/m and maximum sand transport rates of 0.6 m^3 a day. These values are larger than other observed shoreward sand transport rates along the Belgian coast. A long-term analysis (Strypsteen et al., 2019) showed yearly accumulation of 6-12 m^3/m along the Belgian coast but as the beach is sculpted regularly it is difficult to compare the results directly. The

maximum sand transport rate is also difficult to compare as the time scales are different than for example typical obtained values in Belgium (Strypsteen et al., 2021) and the Netherlands (Hoonhout & Vries, 2016).

The scan epochs show a lot of spatio-temporal variations during the one year scan period. These are both natural and anthropogenic variations (i.e. beach shaping). This is also reflected in the large number of objects found in the 4D-OBC analysis. The analysis shows a large number of detected accumulations, but it requires a substantial effort to analyze all accumulations in detail. A new technique has recently been developed by Hulskemper et al. (2022) which could help to further analyze the characteristics of the large number of 4D-OBCs by using self-organizing maps. The technique clusters groups of 4D-OBC with similar properties (like height, size, duration, etc.) and allows for advanced unsupervised identification and characterization of different surface changes. This might, for example, enable to grouping similar accumulations observed in the scan dataset.

CONCLUSION

Near-continuous TLS was used to obtain a one-year dataset of 7.700 laser scans and was analyzed for shoreward sand transport at Mariakerke-Bad. A simplified angle correction method was used to obtain time-dependent scan corrections to account for the varying visibility of the available georeferenced objects.

The scans show consistent but varying sand transport rates through the year towards the seawall with volumes up to 17 m^3/m and shoreward sand transport fluxes of about 0.6 m^3 a day. A large part of this transport is however redistributed at the end of the measuring period due to beach shaping. Alongshore analysis of the shoreward sand transport shows local variations but no clear signs of consistent and significant alongshore aeolian transport.

A total of about 3600 accumulations were found with the 4D-OBC analysis technique. Analysis shows that most accumulations occur with wind speeds above 6-7 m/s and are in the order of centi- to decimeters (suggesting natural processes) and accumulations are found more or less evenly distributed throughout the year

ACKNOWLEDGMENTS

The work in this article was partly financed by the ERC-Advanced grant 291206-Nearshore Monitoring and Modelling, the CoastScan project 2018/STW/00505023, The Crest project (financed by the strategic Basic Research (SBO) program of the Flanders Innovation & Entrepreneurship, Belgium), and contract 4500277210/31141555 of Rijkswaterstaat, Ministry of Infrastructure and Water Management. The authors wish to thank the owner and manager of the Hotel Vayamundo in Mariakerke Bad, Belgium for supporting the research by allowing the use of the hotel infrastructure for the permanent TLS setup. Additional thanks go to Baars-CIPRO (www.baars-cipro.nl) for construction of the measuring frame and financial and operational support.

REFERENCES

Anders, K., Winiwarter, L., Lindenbergh, R., Williams, J.G., Vos, S.E. and Höfle, B. 2020. 4D objects-by-change: Spatiotemporal segmentation of geomorphic surface change from LiDAR time series, *ISPRS Journal of Photogrammetry and Remote Sensing*, 159, 352-363.

Anders K., Winiwarter, L., Mara H., Lindenbergh, R.C., Vos, S.E. and Höfle B. 2021. Fully automatic spatiotemporal segmentation of 3D LiDAR time series for the extraction of natural surface changes, *ISPRS Journal of Photogrammetry and Remote Sensing*, 173, 297-308.

Arens, S.M., van Boxel, J.H. and Abuodha, J.O.Z. 2002, Changes in grain size of sand in transport over a foredune, *Earth Surf. Process. Landforms*, 27, 1163-1175.

Besl P.J. and McKay, N.D. 1992. A method for registration of 3-D shapes. *IEEE Transactions on Pattern Analysis and Machine Intelligence* 14, 239-256.

Brandt, E., Sloover L. de, Wulf, A. de, Montreuil A.L., Vos S.E. and Chen M. 2019. Cross-Shore Suspended Sediment Transport in Relation to Topographic Changes in the Intertidal Zone of a Macro-Tidal Beach (Mariakerke, Belgium), *Journal of Marine Science and Engineerin*g 2019, 7(6), 172.

Brodie K, Conery I, Cohn N, Spore N and Palmsten M. 2019. Spatial Variability of Coastal Foredune Evolution, Part A: Timescales of Months to Years, *Journal of Marine Science and Engineering*, 7, 124.

Duarte-Campos, L., Wijnberg, K.M. and Hulscher, S.J.M.H. 2018. Estimating Annual Onshore Aeolian Sand Supply from the Intertidal Beach Using an Aggregated-Scale Transport Formula, *Journal of Marine Science and Engineering* 6, 127.

Buckley, R. 1996. Effects of Vegetation on the Transport of Dune Sand, *Annals of Arid Zone*, 35, 215-223.

Campos, L.D., Wijnberg, K.M. and Hulscher, S.J.M.H. 2021. Field test of the accuracy of laser particle counters to measure aeolian sediment flux, *Aeolian Research* 50, 100676.

Deruyter, G., De Sloover, L., Verbeurgt, J., De Wulf, A. and Vos, S. E. 2020. Macrotidal Beach Monitoring (Belgium) using Hypertemporal Terrestrial Lidar, *Proceedings FIG Working Week 2020: Smart surveyors for land and water management Amsterdam, the Netherlands, 10–14 May 2020*

Goossens, D., Nolet, C., Etyemezian, V., Campos, L.D., Bakker, G. and Riksen, M. 2018. Field testing, comparison, and discussion of five aeolian sand transport measuring devices operating on different measuring principles, *Aeolian Research* 32, 1-13.

Hage(a), P., Ruessink, G. and Donker, J.J.A. 2018. Determining sand strip characteristics using Argus video monitoring, *Aeolian Research*, 33, 1-11.

Hage(b) P, Ruessink G & Donker J. 2018. Using Argus Video Monitoring to Determine Limiting Factors of Aeolian Sand Transport on a Narrow Beach, *Journal of Marine Science and Engineering* 6, 138.

Hardisty, J. 1994. *Beach and nearshore sediment transport, Sediment transport and depositional processes*, Pye K., Blackwell Sci. Pub., 397. pp.

Hateren, J., Buuren, U. van, Arens, S.M., Balen, R. and van Prins. M. 2019. Identifying sediment transport mechanisms from grain size-shape distributions, *Earth surface dynamics*.

Hesp, P.A, 1999. *The beach backshore and beyond. Handbook of Beach and Shoreface Morphodynamics,* Ed. A.D. Short (Brisbane, Australia), John Wiley and Son, 145-170 pp..

Holman, R.A. and Stanley, J. 2007. The history and technical capabilities of Argus, *Coastal Engineering*, 54, 477–491.

Hoonhout, B. M. and Vries, S. de. 2016. A process-based model for aeolian sediment transport and spatiotemporal varying sediment availability, *Journal of Geophysical Research Earth Surface*, 121, 1555–1575.

Hoonhout, B. & Vries, S. de. 2017. Aeolian sediment supply at a mega nourishment. *Coastal Engineering*, 123. 11-20.

Hulskemper, D., Anders, K., Antolínez, J. A., Kuschnerus, M., Höfle, B., and Lindenbergh, R. C. 2022. Characterization of Morphological Surface Activities Derived from Near-Continuous Terrestrial LIDAR Time Series*, ISPRS-International Archives of the Photogrammetry, Remote Sensing and Spatial Information Sciences*, 48, 53-60.

Intergovernmental Panel on Climate Change (IPCC WGII Sixth Assessment Report). 2022: *Cross-Chapter Paper 2: Cities and Settlements by the Sea* [Garschagen, M., Haasnoot, M., Singh, C., Thomas, A., Aearts, J., Blackburn, S., Catt, D., Chu, E., Solecki, W., Temmerman, S. & Winterer, G.].

Kuschnerus, M., Schröder, D. and Lindenbergh, R.C. 2021. Environmental influences on the stability of a permanently installed laser scanner, *International Archives of the Photogrammetry, Remote Sensing and Spatial Information Sciences*, 43, 745-752.

Lague, D., Brodu, N. and Leroux, J. 2013. Accurate 3D comparison of complex topography with terrestrial laser scanner: Application to the Rangitikei canyon (N-Z), *ISPRS Journal of Photogrammetry and Remote Sensing,* 82.

Luijendijk, A., Hagenaars, G., Ranasinghe, R., Baart, F., Donchyts, G. & Aarninkhof, S.G.J. 2018. The State of the World's Beaches, *Nature Scientific Reports*, 8.

O'Dea, A., Brodie, K. & Hartzell P. 2019. Continuous Coastal Monitoring with an Automated Terrestrial Lidar Scanner, *Journal of Marine Science and Engineering*, 7, 37.

De Sloover, L., Wulf, A., Stal, C., Verbeurgt, J., Vos and Vos, S.E. 2019 Case Study of a Hypertemporal Terrestrial LiDAR to Monitor a Macrotidal Beach: Assessment of Different Calibration Procedures, *19th International Multidisciplinary Scientific GeoConference* SGEM.

Smit, M.W.J., Aarninkhof, S.G.J., Wijnberg, K.M., González, M., Kingston, K.S., Southgate, H.N., Ruessink, B.G., Holman, R.A., Siegle, E., Davidson,M. and Medina, R. 2007. The role of video imagery in predicting daily to monthly coastal evolution, *Coastal Engineering* 54, 539-553.

Strypsteen, G., Houthuys, R. and Rauwoens, P. 2019. Dune Volume Changes at Decadal Timescales and Its Relation with Potential Aeolian Transport, *Journal of Marine Science and Engineering*, 7. 357.

Strypsteen(a), G., Rijn, L.C. van, Hoogland, M.D., Rauwoens, P., Fordeyn, J., Hijma, M.P. & Lodder Q, 2021, Reducing aeolian sand transport and beach erosion by using armour layer of coarse materials, *Coastal Engineering* 166, 103871.

Strypsteen(b), G. S, Rijn, L.C. van & Rauwoens, P. 2021, Comparison of equilibrium sand transport rate model predictions with an extended dataset of field experiments at dry beaches with long fetch distance, *Aeolian Research* 52, 100725.

Swann, C., Lee, D., Trimble, S. & Key, C. 2021, Aeolian sand transport over a wet, sandy beach. *Aeolian Research* 51, 100712.

Meetnet Vlaamse Banken, 2022, location Nieuwpoort. https://meetnetvlaamsebanken.be/, last visited 3/11/2022.

Valentini, E., Taramelli, A., Cappucci, S., Filipponi, F. and Nguyen Xuan, A. 2020. Exploring the Dunes: The Correlations between Vegetation Cover Pattern and Morphology for Sediment Retention Assessment Using Airborne Multisensor Acquisition, *Remote Sensing,* 12, 1229.

Vos, S.E., Lindenbergh, R.C. & Vries, S. de. 2017. CoastScan: Continuous monitoring of coastal change using terrestrial laser scanning. *Proceedings of the 8th International Conference on Coastal Dynamics, Helsingør, Denmark*

Vos, S.E., Spaans, L., Reniers, A., Holman, R., Mccall R. and Vries, S.de. 2020. Cross-Shore Intertidal Bar Behavior along the Dutch Coast: Laser Measurements and Conceptual Model. *Journal of Marine Science and Engineering*, 8, 864.

Vos, S.E., Anders, K.A., Kuschnerus, M., Lindenbergh, R.C., Höfle, B., Aarninkhof, S.G.J and Vries S.de. 2022. A high-resolution 4D terrestrial laser scan dataset of the Kijkduin beach-dune system, The Netherlands. *Nature Scientific Data* 9, 191.

Vousdoukas, M.I., Ranasinghe, R., Mentaschi, L., Plomaritis, T.A., Athanasiou, P., Luijendijk, A. and Feyen L. 2020. Sandy coastlines under threat of erosion. *Nature Climate Change* 10, 260–263.

Vries(a), S. de, Southgate, H.N., Kanning, W. & Ranasinghe, R., 2012, Dune behavior and aeolian transport on decadal timescales, Coastal Engineering 67, 41-53.

Vries(b), S.de, Stive, M.J.F., Rijn, L.van and Ranasinghe, R. 2012, A new conceptual model for aeolian transport rates on beaches, *ICCE 2012: Proceedings of the 33rd International Conference on Coastal Engineering*, 7.

Vries, S.de, Verheijen, A., Hoonhout, B., Vos, S.E., Cohn, N. and Ruggiero, P. 2017. Measured spatial variability of beach erosion due to aeolian processes. *Proceedings of the Coastal Dynamics Conference*. 481-491.

Wiggs, G.F.S, Baird, A.J. and Atherton, R.J, 2004. The dynamic effects of moisture on the entrainment and transport of sand by wind, *Geomorphology* 59, 13-30.